mater.scichina.com link.springer.com

Published online 15 December 2020 | https://doi.org/10.1007/s40843-020-1504-0
Sci China Mater 2021, 64(4): 892–898

MoS_x microgrid electrodes with geometric jumping effect for enhancing hydrogen evolution efficiency

Zhicheng Shang[†], Ying Zhang[†], Liang Luo[*], Congtian Cheng, Tianhui Xie, Fanhong Chen, Siyu Sheng, Yun Kuang, Wen Liu, Haijun Xu[*] and Xiaoming Sun[*]

ABSTRACT Bubble evolution behaviors play important roles in bubble emission reactions. Here we fabricated one-dimensional (1D)-aligned MoS_x microgrids to investigate the influence of the periodic structure on bubble releasing. It is demonstrated that the utilization of the surface energy released during coalescence of bubbles causes them to jump from the electrode, which can be an effective route to eliminate the bubble shielding effect. Under the optimized architecture with 40-μm-wide grooves, the generated bubbles tend to coalesce and release from the electrode with much smaller size (65% less in volume). By balancing the coalescence efficiency and the adhesive work *via* the architecture engineering, the electrocatalytic performance can be promoted with the rapid bubble removal and lowered ohmic resistance. The results provide new insights into the rational design of novel catalytic electrode architectures and promote their applications in related fields.

Keywords: bubble evolution, coalescence, surface energy

INTRODUCTION

Electrochemical gas evolution reactions (GERs), such as oxygen evolution reaction (OER), hydrogen evolution reaction (HER) and chlorine evolution reaction (ClER) hold the key for developing renewable energy conversion and storage technologies of fuel cells [1], water splitting [2,3], and metal-air batteries [4]. To achieve high energy efficiency of these processes, fast reaction kinetics is desperately desired. Apart from the intrinsic performance of catalysts [5–9], gas behaviors on the electrode surface are known to influence the mass transfer in GER [10,11]. As a huge amount of bubbles are generated in short time at high current densities [12], the large adhesive force of gas bubbles would lead to the formation of a bubble layer, covering the active sites, increasing ohmic resistance and deteriorating the total activity of the catalysts [13–16]. This denying phenomenon, termed as "bubble shielding effect", takes place at the catalytic electrode surface and lowers the electrolysis efficiency [17].

To eliminate the bubble shielding effect, superwettability has been developed to reduce the bubble size by introducing discontinuous three-phase contact line (TPCL) to decrease the adhesive force. We and other groups [16,18,19] have developed nanoarray-based catalysts with superhydrophilicity for GERs [10,17,20,21] and superhydrophobicity for gas consumption reactions (GCRs) [22,23]. Such superwetting structures result in significantly enhanced total activity and stability [16]. However, rational design of surface architectures of next-generation electrodes still remains rather vague, due to the lack of fundamental understanding, especially from quantitative point of view. To develop new strategy for further optimization is of vital significance [24–27].

Marvellous interfaces with biomimetic architectures have been fabricated and demonstrated their features [19,28–30]. As one of the anti-icing strategies, it has been found that the adjacent bubbles can jump away from the surface at certain velocities as assisted by surface energy released during bubble coalescence, which is partly converted into the out-of-plane kinetic energy (due to symmetry breaking) [31]. Previous studies on such coalescence-induced jumping mainly focused on droplets, demonstrating that the efficiency was related to the coalesced droplet number, droplet-size-dependent surface adhesion, and pinning state [15,29]. While for numerous bubbles generated in GERs, such coalescence should induce far more jumping than the droplet counterparts and benefit the elimination of bubble shielding effect.

State Key Laboratory of Chemical Resource Engineering, Beijing Advanced Innovation Centre for Soft Matter Science and Engineering, Beijing University of Chemical Technology, Beijing 100029, China
[†] These authors contributed equally to this work.
[*] Corresponding authors (emails: luoliang@mail.buct.edu.cn (Luo L); hjxu@mail.buct.edu.cn (Xu H); sunxm@mail.buct.edu.cn (Sun X))

Herein, we fabricated a series of one-dimensional (1D)-aligned MoS_x microarray electrodes with varied groove widths to investigate the influence of coalescence-induced jumping for improving the electrochemical hydrogen bubble evolution (Fig. 1). With the merits of architectures, the generated bubbles tend to coalesce and overcome the adhesive work of the electrode with much smaller size driven by the surface energy. The coalescence efficiency can be tuned by the groove width, significantly lowering the bubble shielding effect and the ohmic resistance and promoting the electrocatalytic performance. The results provide new insights into the rational design of novel catalytic electrode architectures as well as other bubble evolution applications.

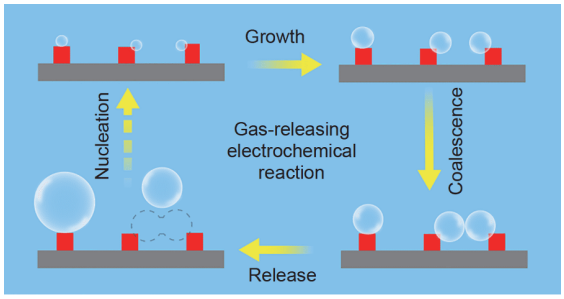

Figure 1 Schematic illustration of the underwater bubble coalescence and release.

EXPERIMENTAL SECTION

The original silicon wafer patterns with precise sizes were obtained by photolithographic technology. The embossment widths and the groove depths were 10 μm conformably, and the groove widths were 20, 40, 60 and 80 μm, respectively. The first step was to make the elastic stamp, prepared by mixing polydimethylsiloxane (PDMS) with SYLGARD 184A and SYLGARD 184B (10:1). After mixing PDMS and curing agent uniformly, the PDMS was placed still for 30 min to remove inner gas bubbles. Then the PDMS was cast on the antecedent silicon wafer patterns and dried in oven at 60°C for 5 h. The solidified PDMS was peeled from the silicon wafer patterns to form the replica. The MoS_x precursor was prepared by adding 50 mg of $(NH_4)_2MoS_4$ into 5 mL of *N*,*N*-dimethyl formamide (DMF) and then sonicating for 30 min. Ti substrates (2 cm × 2 cm) were sonicated in concentrated HCl solution (~37 wt%) and rinsed with deionized water and ethanol for 5 min, respectively, and dried at 80°C for 30 min. After placing PDMS molds on the Ti substrates, 50 μL of $(NH_4)_2MoS_4$ solution was dropped around the stamp edge and infiltrated into the channels by capillary effect twice, and dried by freeze-drying for 3 h, respectively. The PDMS stamps were then stripped from the substrates gently. Finally, the samples were annealed at 170°C for 30 min in a tube furnace under Ar atmosphere to form the patterned MoS_x electrode.

Field-emission scanning electron microscope (SEM; Zeiss SUPRA 55) operated at 20 kV was used to characterize the size and morphology of the samples. The adhesive force between gas bubbles and the surface of electrodes was tested by a high-sensitivity micro-electromechanical balance system (Dataphysics DCAT21, Germany). An optical microscope and a charge-coupled device (CCD) system were used to take photographs at the rate of one frame per second. The electrode surface was placed in a square quartz cell (5 cm × 5 cm × 5 cm) filled with 0.5 mol L^{-1} H_2SO_4 (electrolyte) and the cell was fixed to the plate of the balance system. The force of this balance system was initially set to zero and then a gas bubble (~2 μL) was suspended on a metal ring in the 0.5 mol L^{-1} H_2SO_4. The electrode was moved upward at a constant speed of 0.01 mm s^{-1} until the surface contacted with the gas bubbles. The force value increased gradually until reaching its maximum and the shape of the gas bubble changed from spherical to elliptical. When the electrode moved down further, the contact was sharply reduced to near zero and the shape of the gas bubbles changed back to spherical.

The bubble contact angle was evaluated by the captive bubble method (Data physics OCA20) and was defined as the observed equilibrium contact angle of liquid around the pinned bubbles on a solid surface, where the liquid/gas interface met the solid/liquid interface across the three-phase contact interfaces. The volume of the gas bubble was about 2 μL for each testing. All experiments were repeated for more than five times.

Hydrogen bubble releasing process was measured by a CCD-mounted microscope (SZ-CTC, OLYMPUS) for continuous imaging. The illumination was obtained by a fiber optic illuminator system (Multi-Position, Nikon). The electrochemical measurements were carried out at room temperature in a three-electrode glass cell connected to an electrochemical workstation (CHI 660D, Chenghua, Shanghai). The working electrode was the as-prepared patterned electrode, and carbon paper was used as the counter electrode and a silver/silver chloride electrode was used as the reference electrode. H_2SO_4 solution (0.5 mol L^{-1}) was used as the electrolyte. The HER was conducted under the current density of 2 mA cm^{-2}. Prior to the measurements, hydrogen was bubbled into the electrolyte solution to eliminate the dissolved oxygen and

to maintain a fixed Nernst potential for the H^+/H_2 redox couple. Linear sweep voltammetry (LSV) with a scan rate of 5 mV s^{-1} and alternative current (AC) impedance measurements were carried out in the same configuration at the potential of −0.4 V from 10^5 to 0.1 Hz with voltage amplitude of 5 mV.

RESULTS AND DISCUSSION

As demonstrated in Fig. 2a, the 1D aligned structure was achieved by the patterning technology called micro-moulding in capillaries (MIMIC) on Ti substrate [32,33]. PDMS was firstly cast on a silicon wafer with photolithographic patterning including precise sizes and solidified to form a pattern replica [34]. The as-formed PDMS replica was stamped on a Ti substrate to form continuous capillary channels. $(NH_4)_2MoS_4$ solution as the precursor was dropped on one end of the channels until it filled into the channels by capillary force; after removing the PDMS replica, the structured electrode was obtained after calcination at 170°C for 30 min. SEM image and the corresponding energy dispersive X-ray spectroscopy (EDS) indicate that Mo and S elements distributed along the array structures (Fig. S1) and X-ray photoelectron spectroscopy (XPS) spectra confirm the formation of MoS_x with the Mo:S ratio of 0.4 (Fig. S2). The groove widths of MoS_x microarrays were chosen to be 20, 40, 60 and 80 μm and the embossment width and the groove depth were 10 μm.

Fig. 2b–e show the schematic illustration of MoS_x microarrays with four different groove widths (20, 40, 60 and 80 μm), and the top-view SEM images (Fig. 2f–i) and digital images (Fig. 2j–m) verify the periodic structures with different intervals. Thanks to the periodic patterned rough surface structure [35], the bubble contact angles on all the four electrodes were greater than 130°, as shown in Fig. S3. The side-upper schematic images in Fig. S3 indicate the distinct discontinuous state of the TPCL of a bubble of ~ 2 μL on the four kinds of MoS_x patterns with different groove widths. As the groove width increased from 20 to 80 μm, the corresponding adhesive force of bubbles decreased from 32 to 5.8 μN.

With the aligned structure, the generated bubbles were able to coalesce and jump from the electrode, similar to the liquid drops bounded off by coalescence on the anti-icing surfaces [28]. An optical microscope with a CCD camera system was used to snapshot the processes of gas bubble formation, growth, coalescence and release during HER with a three-electrode system, as shown in Fig. 3. All videos/images were taken at the same time interval with relatively low current density (−2 mA cm^{-2}) to ensure the clarity of bubble releasing behaviors. Due to the coalescence of two small bubbles into a bigger one and the induced jumping effect (red dashed circles), the detachment size of bubbles with coalescence was essentially smaller than that without coalescence.

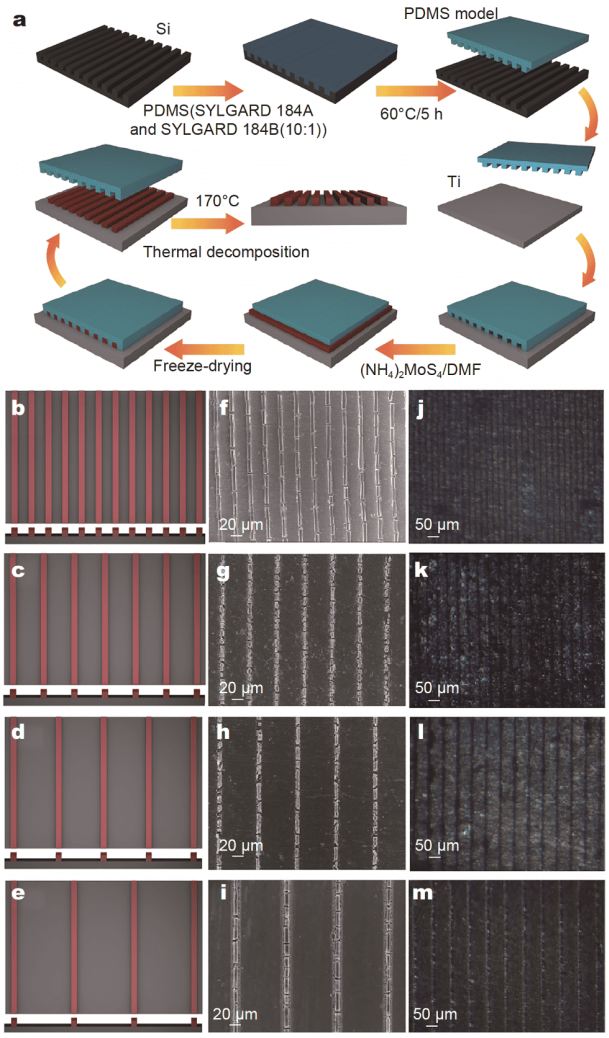

Figure 2 (a) Schematic illustration of the patterning of MoS_x microarrays on Ti substrate achieved by MIMIC. Schematic cartoons of the top-view and side-view of different periodic groove widths of (b) 20 μm, (c) 40 μm, (d) 60 μm and (e) 80 μm. SEM images of MoS_x micro-arrays with different periodic groove widths of (f) 20 μm, (g) 40 μm, (h) 60 μm and (i) 80 μm. Digital images of the typical top-view of MoS_x microarrays with different periodic groove widths of (j) 20 μm, (k) 40 μm, (l) 60 μm and (m) 80 μm.

Typically, for the electrode with 20 μm groove width, the size for coalescence-induced detachment was found to be 50 ± 10 μm, whereas that without coalescence was 80 ± 10 μm. Similarly, H_2 bubbles released by coalescence with grooves of 40, 60 and 80 μm in width were 60 ± 10,

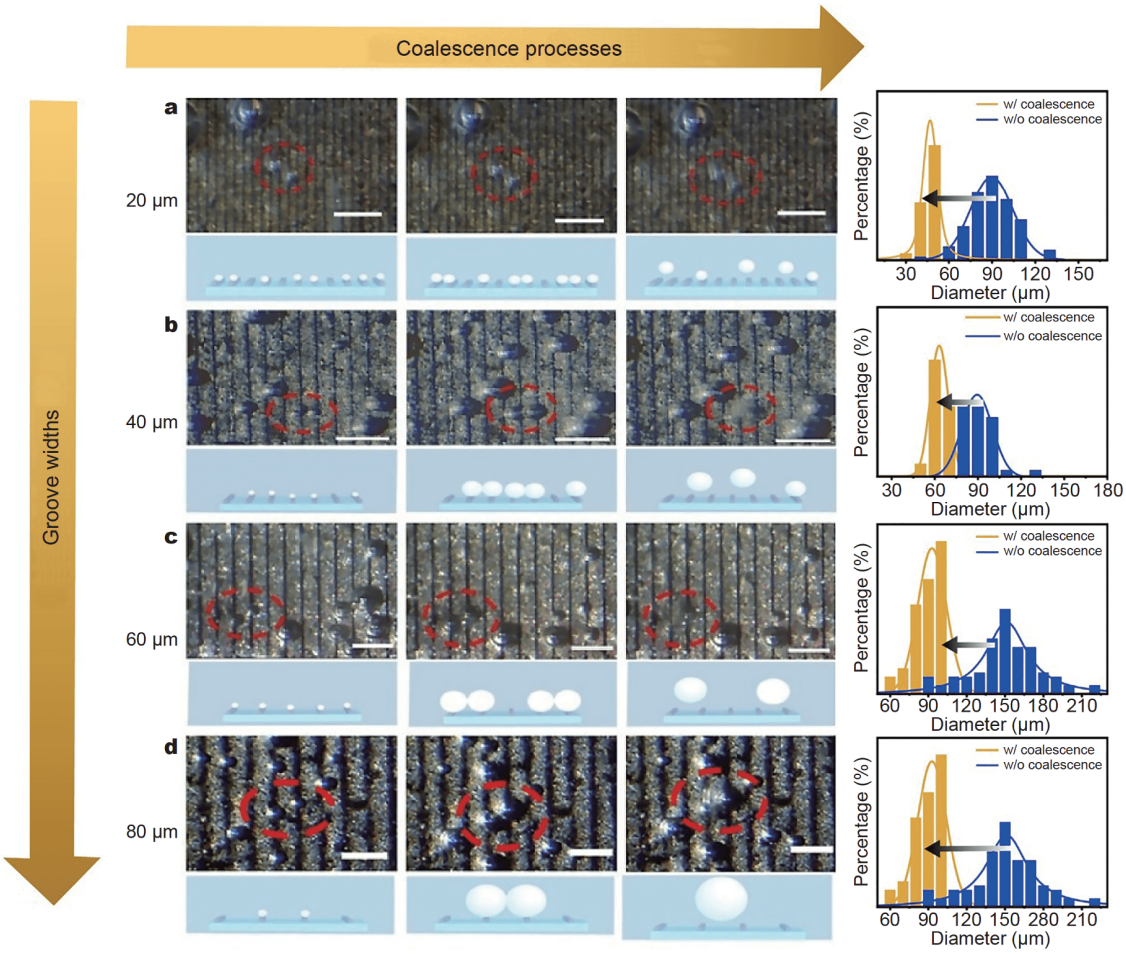

Figure 3 Digital images of different bubble behaviors and their corresponding statistics of size distribution of the released bubbles on MoS_x microarrays with different periodic groove widths of (a) 20 μm, (b) 40 μm, (c) 60 μm and (d) 80 μm (scale bar: 150 μm).

80 ± 10 and 100 ± 10 μm in diameter, respectively. They were ~ 65% less in volume relative to the bubbles without coalescence, which were 90 ± 10, 130 ± 10 and 150 ± 10 μm in diameter, respectively. The above results demonstrate that the coalescence-induced jumping effect can promote the detachment of bubbles when they were still small.

Such bubble behaviors significantly influenced the electrocatalytic HER performance. The effect of bubble detachment on polarization curves was firstly confirmed on the same electrode with different orientations. The polarization curves recorded on the same electrode with two different directions based on the same line-patterned MoS_x nanoarrays were compared, as shown in Fig. 4a. As the electrode was put into the electrolyte vertically (namely, the groove direction was parallel to the buoyancy direction), the bubbles rolled up along the grooves, coalesced and released efficiently. In contrast, when the electrode was placed vertically with the groove direction perpendicular to the buoyancy direction, the generated bubbles would have to grow big enough to overcome the "stages", leading to much slower current increase rate. The results clearly prove the bubble effect on the performance.

The groove width would affect the efficiency of coalescence and the consequent current increase rate. To further clarify the coalescence efficiency, the polarization curves of the four electrodes were compared in 0.5 mol L^{-1} H_2SO_4 solution with *i*R correction (Fig. 4b), as well as the electrochemical surface area and theoretical physical surface area (Fig. S4). The onset potentials for all the four MoS_x electrodes were the same (−0.13 V), as the same intrinsic activity. But with different bubble detachment behaviors, as we expected, the electrode with 40 μm groove width exhibited the fastest increase of cathodic current density with the slope (current density:

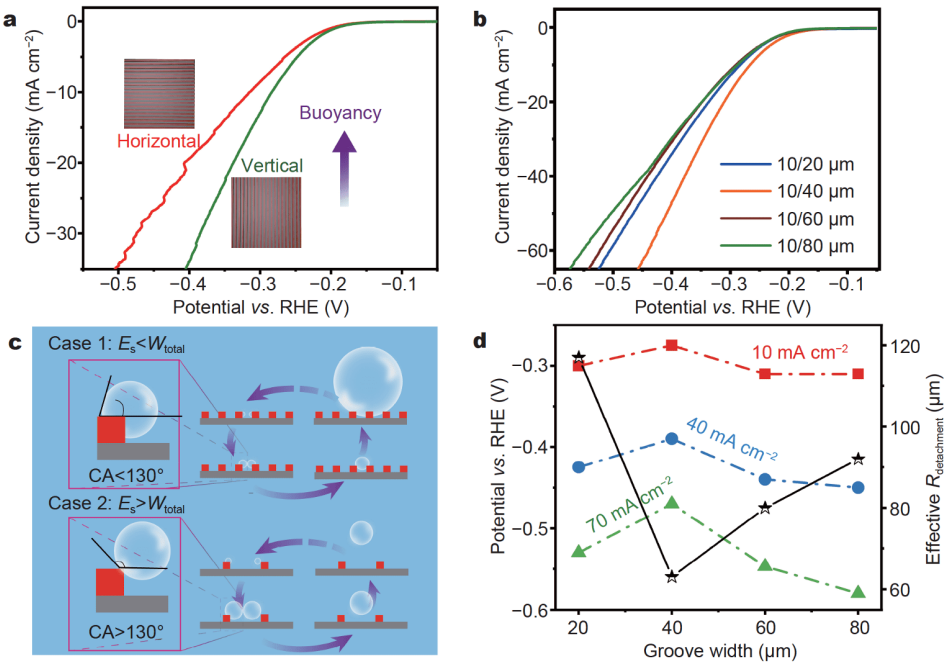

Figure 4 (a) Polarization curves obtained for 90° (vertical) and 0° (horizontal) MoS_x array electrodes with groove width of 40 μm. (b) Polarization curves obtained from patterned MoS_x electrodes with different periodic groove widths of 20, 40, 60 and 80 μm. (c) Scheme of two different bubble behaviors. (d) Plots of overpotential variation and the effective radius for bubble detachment on different groove widths.

potential) of 0.32 mA mV^{-1}, which is 1.2, 1.2 and 1.5 times higher than that of 20 μm (0.26 mA mV^{-1}), 60 μm (0.26 mA mV^{-1}) and 80 μm (0.21 mA mV^{-1}) groove electrodes corresponding with detachment behaviors of smaller bubbles. Moreover, it also exhibited smaller resistance (19 Ω) than that of the electrodes with 20 μm (24 Ω), 60 μm (24 Ω) and 80 μm (37 Ω) groove width, as evidenced by the electrochemical impedance spectroscopy (EIS) studies (Fig. S5).

It is clear that the coalescence would induce bubble jumping (Scheme S1) as the released surface energy (E_s) can overcome the total adhesion work of two bubbles (W_{total}), namely, $E_s > W_{total}$. According to the calculation (see more details in Note S1, Supplementary information), the key point was found to be only related to the contact angle of the two generated bubbles on two adjacent grooves before the coalescence. As we assumed the two bubbles were with the same size, the critical value of contact angle was 130°. Typically, the electrode with the 20 μm groove width had the smallest theoretical coalescence bubble size, but the generated bubbles on the given grooves could not grow big enough and move to the top surface with the contact angle larger than 130° (Fig. 4c, Case 1). As a result, the surface energy released during coalescence could hardly be higher than the adhesion work of two bubbles and the coalesced bubble would keep growing till big enough to detach from the electrode by finally overcoming the adhesion force. The ineffective coalescence on the electrode with 20 μm groove width caused the practical detached bubble size much bigger than the just coalesced size, even as the biggest among the four electrodes due to the largest adhesion force. For the other cases, the larger width provided enough space for bubbles to grow big enough on the grooves and the contact angle could reach up to greater than 130° before the coalescence (Fig. 4c, Case 2). Hence, the coalesced bubble would jump away from the electrodes effectively for the electrodes with groove widths of 40, 60 and 80 μm. While the increase of groove width would cause the reduction of the electrochemical active surface area (Scheme S2). By balancing the coalesced efficiency and the electrochemical active surface area, the average bubble size for detachment on the electrode with 40 μm groove width was the smallest, which thereby exhibited superior performance than the other three electrodes, particularly the smallest overpotential (−0.26 V) than the others at the current density of −10 mA cm^{-2}. Moreover, the bubble effect became more and more significant at high current densities. As the current density increased to −40 and −70 mA cm^{-2}, such overpotential difference (0.13 V) be-

came more obvious owing to the severe bubble shielding effect at high current densities (Fig. 4d). The results indicate that the coalescence-induced jumping strategy would be a promising route to promote bubble removal and GER performance.

CONCLUSIONS

In summary, MoS_x microarray electrodes with 1D-aligned pattern were fabricated to investigate the influence of the periodic structure on bubble releasing. It was found that the generated bubbles would coalesce and jump from the electrodes with much smaller size (~65% less in volume) driven by the surface energy released during coalescence. The coalescence efficiency can be tuned by the variation of groove width and the groove width of 40 μm exhibited superior HER performance than the other widths, owing to the well balance between enough surface energy change and adhesion work of substrate and larger electrochemical surface active area. Such coalescence-induced bubble release not only lowers the bubble shielding effect to promote the catalytic performance, but also provides new insights into the rational design of architectures of catalytic electrodes in emerging devices.

Received 17 July 2020; accepted 24 August 2020; published online 15 December 2020

1 Seh ZW, Kibsgaard J, Dickens CF, *et al.* Combining theory and experiment in electrocatalysis: Insights into materials design. Science, 2017, 355: eaad4998
2 Guo K, Wang Y, Yang S, *et al.* Bonding interface boosts the intrinsic activity and durability of NiSe@Fe_2O_3 heterogeneous electrocatalyst for water oxidation. Sci Bull, 2020, doi: 10.1016/j.scib.2020.06.003
3 Zhang Y, Shi M, Wang C, *et al.* Vertically aligned NiS_2/CoS_2/MoS_2 nanosheet array as an efficient and low-cost electrocatalyst for hydrogen evolution reaction in alkaline media. Sci Bull, 2020, 65: 359–366
4 Cheng F, Chen J. Metal-air batteries: From oxygen reduction electrochemistry to cathode catalysts. Chem Soc Rev, 2012, 41: 2172–2192
5 Om Bockris J. A hydrogen economy. Science, 1972, 176: 1323
6 Turner JA. Sustainable hydrogen production. Science, 2004, 305: 972–974
7 Jamesh MI, Sun X. Recent progress on earth abundant electrocatalysts for oxygen evolution reaction (OER) in alkaline medium to achieve efficient water splitting: A review. J Power Sources, 2018, 400: 31–68
8 Li X, Rong H, Zhang J, *et al.* Modulating the local coordination environment of single-atom catalysts for enhanced catalytic performance. Nano Res, 2020, 13: 1842–1855
9 Zhuang Z, Kang Q, Wang D, *et al.* Single-atom catalysis enables long-life, high-energy lithium-sulfur batteries. Nano Res, 2020, 13: 1856–1866
10 Xu W, Lu Z, Sun X, *et al.* Superwetting electrodes for gas-involving electrocatalysis. Acc Chem Res, 2018, 51: 1590–1598
11 Mohammed-Ibrahim J, Sun X. Recent progress on earth abundant electrocatalysts for hydrogen evolution reaction (HER) in alkaline medium to achieve efficient water splitting: A review. J Energy Chem, 2019, 34: 111–160
12 Li Y, Zhang H, Jiang M, *et al.* 3D self-supported Fe-doped Ni_2P nanosheet arrays as bifunctional catalysts for overall water splitting. Adv Funct Mater, 2017, 27: 1702513
13 Wang M, Wang Z, Gong X, *et al.* The intensification technologies to water electrolysis for hydrogen production: A review. Renew Sustain Energy Rev, 2014, 29: 573–588
14 Mazloomi SK, Sulaiman N. Influencing factors of water electrolysis electrical efficiency. Renew Sustain Energy Rev, 2012, 16: 4257–4263
15 Shi Y, Zhang B. Recent advances in transition metal phosphide nanomaterials: Synthesis and applications in hydrogen evolution reaction. Chem Soc Rev, 2016, 45: 1529–1541
16 Lu Z, Zhu W, Yu X, *et al.* Ultrahigh hydrogen evolution performance of under-water "superaerophobic" MoS_2 nanostructured electrodes. Adv Mater, 2014, 26: 2683–2687
17 Xu W, Lu Z, Wan P, *et al.* High-performance water electrolysis system with double nanostructured superaerophobic electrodes. Small, 2016, 12: 2492–2498
18 Wang Q, Chen S, Shi F, *et al.* Structural evolution of solid Pt nanoparticles to a hollow PtFe alloy with a Pt-skin surface *via* space-confined pyrolysis and the nanoscale Kirkendall effect. Adv Mater, 2016, 28: 10673–10678
19 Song Q, Xue Z, Liu C, *et al.* General strategy to optimize gas evolution reaction *via* assembled striped-pattern superlattices. J Am Chem Soc, 2020, 142: 1857–1863
20 Wang H, Zhang X, Wang J, *et al.* Puffing quaternary $Fe_xCo_yNi_{1-x-y}P$ nanoarray *via* kinetically controlled alkaline etching for robust overall water splitting. Sci China Mater, 2020, 63: 1054–1064
21 Su B, Tian Y, Jiang L. Bioinspired interfaces with superwettability: From materials to chemistry. J Am Chem Soc, 2016, 138: 1727–1748
22 Wu G, Wang J, Ding W, *et al.* A strategy to promote the electrocatalytic activity of spinels for oxygen reduction by structure reversal. Angew Chem Int Ed, 2016, 55: 1340–1344
23 Lu S, Zhuang Z. Electrocatalysts for hydrogen oxidation and evolution reactions. Sci China Mater, 2016, 59: 217–238
24 Jiang J, Li Y, Liu J, *et al.* Recent advances in metal oxide-based electrode architecture design for electrochemical energy storage. Adv Mater, 2012, 24: 5166–5180
25 Zamuruyev KO, Bardaweel HK, Carron CJ, *et al.* Continuous droplet removal upon dropwise condensation of humid air on a hydrophobic micropatterned surface. Langmuir, 2014, 30: 10133–10142
26 Perez-Toralla K, Konda A, Bowen JJ, *et al.* Rational synthesis of large-area periodic chemical gradients for the manipulation of liquid droplets and gas bubbles. Adv Funct Mater, 2018, 28: 1705564
27 Wang L, Xiao FS. A significant enhancement of catalytic performance by adjusting catalyst wettability. Sci China Mater, 2018, 61: 1137–1142
28 Zhang Q, He M, Chen J, *et al.* Anti-icing surfaces based on enhanced self-propelled jumping of condensed water microdroplets. Chem Commun, 2013, 49: 4516–4518
29 Hao C, Liu Y, Chen X, *et al.* Bioinspired interfacial materials with enhanced drop mobility: From fundamentals to multifunctional applications. Small, 2016, 12: 1825–1839
30 Wang S, Liu K, Yao X, *et al.* Bioinspired surfaces with superwettability: New insight on theory, design, and applications. Chem Rev, 2015, 115: 8230–8293
31 Vahabi H, Wang W, Mabry JM, *et al.* Coalescence-induced jumping of droplets on superomniphobic surfaces with macro-

texture. Sci Adv, 2018, 4: eaau3488
32 Xia Y, Rogers JA, Paul KE, *et al.* Unconventional methods for fabricating and patterning nanostructures. Chem Rev, 1999, 99: 1823–1848
33 Vonhören B, Langer M, Abt D, *et al.* Fast and simple preparation of patterned surfaces with hydrophilic polymer brushes by micromolding in capillaries. Langmuir, 2015, 31: 13625–13631
34 Kim E, Xia Y, Whitesides GM. Micromolding in capillaries: Applications in materials science. J Am Chem Soc, 1996, 118: 5722–5731
35 Lai Y, Huang J, Cui Z, *et al.* Recent advances in TiO_2-based nanostructured surfaces with controllable wettability and adhesion. Small, 2016, 12: 2203–2224

Acknowledgements We thank Prof. Lin W and Prof. Dai H for their helpful discussion. This work was supported by the National Natural Science Foundation of China (21675007, 21676015, 21520102002, 91622116 and 22005022), the National Key Research and Development Project (2018YFB1502401 and 2018YFA0702002), the Royal Society and Newton Fund through Newton Advanced Fellowship award (NAF\R1 \191294), the Program for Changjiang Scholars and Innovation Research Team in the University (IRT1205), the Fundamental Research Funds for the Central Universities and the long-term subsidy mechanism from the Ministry of Finance and the Ministry of Education of China.

Author contributions Shang Z, Zhang Y, Luo L, Xu H and Sun X designed and engineered the samples; Shang Z and Zhang Y performed the experiments; Shang Z, Zhang Y, Luo L, Xu H and Sun X wrote the manuscript; Cheng C and Kuang Y assisted the electrocatalytic tests; Xie T and Chen F assisted the theoretical analysis; Sheng S assisted the illustrations; Liu W, Kuang Y and Xie T assisted in revising the manuscript; Sun X, Xu H and Luo L co-supervised the project. All authors contributed to the general discussion.

Conflict of interest The authors declare that they have no conflict of interest.

Supplementary information Experimental details and supporting data are available in the online version of the paper.

Zhicheng Shang is now pursuing his master degree under the supervision of Prof. Xiaoming Sun at the State Key Laboratory of Chemical Resource Engineering, College of Chemistry, Beijing University of Chemical Technology. His current research mainly focuses on interface wettability, synthesises of inorganic nanostructures and *in situ* characterization of electrocatalysis.

Ying Zhang achieved her master degree from the State Key Laboratory of Chemical Resource Engineering, College of Chemistry, Beijing University of Chemical Technology in 2018. Her current research mainly focuses on interface wettability, synthesis of inorganic nanostructures and *in situ* characterization of electrocatalysis.

Liang Luo achieved his BSc degree in 2005 from Beijing Normal University and his PhD degree in 2010 from Fujian Institute of Research on the Structure of Matter, Chinese Academy of Sciences. He joined Beijing University of Chemical Technology in 2010. His current research interest mainly focuses on the synthesis and separation of nanomaterials and *in situ* characterization of electrocatalysis.

Haijun Xu achieved his BSc and PhD degrees from Zhengzhou University in 2002 and 2008, respectively. He joined Beijing University of Chemical Technology in 2008. His current research interest mainly focuses on noble-metal-based surface enhanced Raman scattering for early and rapid detection of disease, high-efficiency organic-inorganic composite solar cells, electroluminescent materials and properties.

Xiaoming Sun achieved his BSc and PhD degrees from Tsinghua University in 2000 and 2005, respectively. He worked at Stanford University as a postdoc from 2005. He joined Beijing University of Chemical Technology in 2008. His current research interest mainly focuses on the synthesis and separation of nanomaterials and improving the energy related electrocatalysis process by tailoring the compositions, surface wettability and micro-/nanostructures.

多硫化钼微网格电极的几何弹跳效应对析氢效率提高的研究

商志成[†], 张英[†], 罗亮[*], 成聪田, 谢天慧, 陈凡红, 盛思雨, 邝允, 刘文, 许海军[*], 孙晓明[*]

摘要 气泡的析出行为在电化学析气反应中具有重要作用. 为了研究周期性结构对气泡脱离的影响, 我们构建了一维线性构造的多硫化钼微网格电极. 结果表明, 利用该电极上的气泡融合行为释放出的表面能可诱导气泡弹起, 从而实现气泡的快速脱离, 消除气泡屏蔽效应. 基于优选的40 μm凹槽宽度, 产生的气泡以融合的方式可使得脱附尺寸显著降低(体积减小65%). 通过结构调控权衡融合效率和黏附功, 可以提升气泡脱附效率, 进而降低欧姆电阻, 提升电催化性能. 该研究结果为新型催化电极结构的合理设计提供了新思路, 促进了催化电极在相关领域的应用.

